

# Optical Properties of Strained Graphene

Vitor M. Pereira,<sup>1</sup> R. M. Ribeiro,<sup>2</sup> N. M. R. Peres,<sup>2</sup> and A. H. Castro Neto\*<sup>1</sup>

<sup>1</sup>Graphene Centre and Department of Physics, National University of Singapore, 2 Science Drive 3, Singapore 117542

<sup>2</sup>Centro de Física e Departamento de Física, Universidade do Minho, P-4710-057, Braga, Portugal

(Dated: November 10, 2020)

The optical conductivity of graphene strained uniaxially is studied within the Kubo-Greenwood formalism. Focusing on inter-band absorption, we analyze and quantify the breakdown of universal transparency in the visible region of the spectrum, and analytically characterize the transparency as a function of strain and polarization. Measuring transmittance as a function of incident polarization directly reflects the magnitude and direction of strain. Moreover, direction-dependent selection rules permit identification of the lattice orientation by monitoring the van-Hove transitions. These photoelastic effects in graphene can be explored towards atomically thin, broadband optical elements.

PACS numbers: 78.67.Wj, 81.05.ue, 73.22.Pr

## I. INTRODUCTION

Transparent flexible electronics is currently a much sought technology, with applications that can range from foldable displays and electronic paper, to transparent solar cells. Graphene, on account of its ultimate thickness, large transparency [1], high mechanical resilience under strong stress/bending cycling, and excellent electronic mobility [2], has been promptly ranked among the best placed materials to achieve those technologies [3, 4]. Such goals require a thorough understanding of the interplay between the different aspects that will unavoidably be present in such devices, namely how sensitive the dielectric and optical properties of graphene are to gating and straining. At the same time, broadband optical elements that can be scaled down to the nanoscale, and easily integrated into photonic/photoelectronic circuits, are equally appealing scenarios in current nanotechnology.

The optical absorption response of graphene has been recently given thorough attention on both the experimental [1, 5–8] and theoretical fronts [9–17]. One of the distinguishing features of undoped (or lightly doped) graphene arises from the constancy of its transparency,  $\mathcal{T}(\omega)$ , which is controlled by electron-hole excitation processes, and universal:  $\mathcal{T}(\omega) \approx 1 - \pi\alpha$  ( $\alpha \simeq 1/137$  being the fine structure constant) [1]. This universality is a consequence of the particle hole symmetry of graphene's spectrum, combined with the cancellation of the frequency dependencies of the matrix element and vanishing density of states. It holds throughout a broad spectral range comprising the frequencies between the Fermi energy,  $\mu$ , and the vicinity of the van Hove singularity (VHS) at the  $M$  point in the Brillouin zone (BZ). In undoped graphene this covers a band spanning the visible region, down to the far IR.

Here we analyze and quantify how the optical ab-

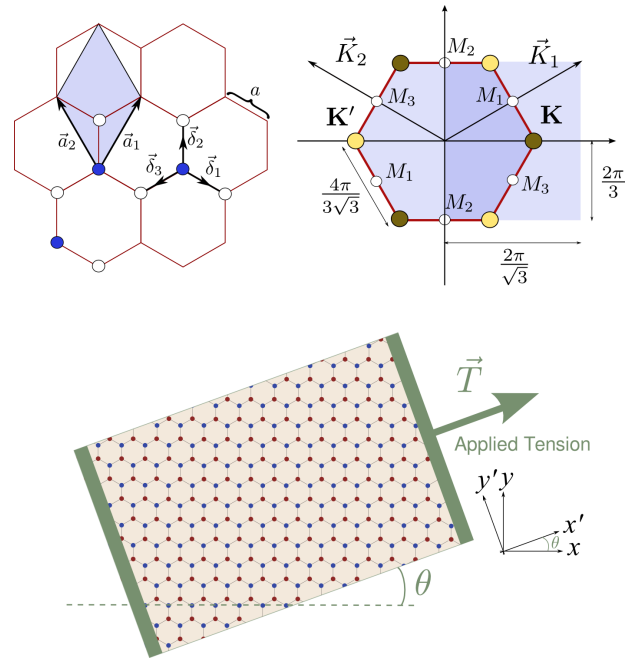


FIG. 1: Lattice orientation in direct and reciprocal space, overlaid with several quantities used in the text. The bottom illustration shows the relative orientation of the lattice with respect to a general tension direction  $\theta$ .

sorption associated with direct optical transitions is affected by strain. The strain-induced anisotropy leaves a clear signature in the optical response of the system, modulating its transmittance, reflectance and absorption, while simultaneously rotating the polarization of incoming light. Tailoring of graphene systems on the basis of such properties extends the concept of strain engineering in graphene from electronic structure and transport [18, 19] to the optical domain as well. Such effects are described next. Related work on effects of strain in graphene's optical response has been reported in Refs. [20–22].

\*On leave from Physics Department, Boston University.

## II. STRAIN-INDUCED ANISOTROPY

We concentrate on uniform uniaxial deformations of free graphene, which provide the highest degree of anisotropy for given amount of strain,  $\varepsilon$ . Within a tight-binding approximation for the  $\pi$ -band subsystem, strain impacts electronic motion via the modification of the Slater-Koster parameters  $t_i \equiv t(\delta_i)$  in the Hamiltonian

$$H = \sum_{\mathbf{R}, \delta} t(\delta) a_{\mathbf{R}}^\dagger b_{\mathbf{R}+\delta} + \text{H. c.} \quad (1)$$

Here  $\mathbf{R}$  denotes a position in the Bravais lattice;  $\delta_{1,2,3}$  connects site  $\mathbf{R}$  to its neighbors;  $a(\mathbf{R})$  and  $b(\mathbf{R})$  are the field operators in sublattices A and B. In what follows, we characterize the interplay between strain and electronic structure in the same framework described in detail in ref. 23. In summary, this entails the assumption that hopping amplitudes vary with distance as  $t(r) \simeq te^{-\lambda(r-a)}$ , with  $t \approx 2.7$  eV,  $a = 1.42$  Å,  $\lambda a \approx 3 - 4$  [21, 23], and we disregard bond bending effects, since they are not significant in this effective description [24]. Bond deformations are uniform and given to linear order in terms of the strain tensor  $\varepsilon_{ij}$ :  $\delta = (\mathbf{1} + \varepsilon) \cdot \delta^0$ . This approximation was shown to describe with good accuracy both the threshold deformation for the Lifshitz and metal-insulator transition at large deformations [23, 25, 26], and the behavior of  $t_i(\delta)$  when compared to *ab-initio* calculations [24]. Since the hexagonal lattice is elastically isotropic,  $\varepsilon_{ij}$  can be fully parametrized by the amount of uniaxial strain,  $\varepsilon$ , its direction  $\theta$  with respect to a zig-zag ( $\mathcal{ZZ}$ ) direction, and Poisson's ratio,  $\nu \approx 0.16$  [23]. Our Cartesian directions are such that a  $\mathcal{ZZ}$  edge coincides with the  $x$  axis (fig. 1). Tension along  $\theta = 0$  [ $\mathcal{ZZ}$ ] and  $\theta = \pi/2$  [armchair ( $\mathcal{AA}$ )] defines representative directions that will be recalled frequently. We shall disregard the strain-induced modification of the reciprocal lattice, as it is not relevant for the optical absorption. Since here we are not interested in large deformations, we further approximate  $t_i \equiv t(\delta_i) \approx t - t\lambda(\delta_i - a)$ .

The low energy Hamiltonian appropriate for optical processes below the UV can be derived conventionally [16], by expanding (1) around the *shifted* Dirac points:  $\mathbf{k} = \mathbf{k}_D + \mathbf{q}$  ( $q \ll k_D$ ). For arbitrary  $t_i$  the nonequivalent Dirac points lie at  $\mathbf{k}_{D,\zeta} = \zeta(A - B, A + B)$ , with  $A = \frac{1}{\sqrt{3}a} \cos^{-1} \frac{t_1 - t_2^2 - t_3^2}{2t_2t_3}$ ,  $B = \frac{1}{3a} \cos^{-1} \frac{t_3^2 - t_1^2 - t_2^2}{2t_1t_2}$ , and  $\zeta = \pm 1$  is the valley index, labeling the two nonequivalent Dirac points. In their vicinity, the electronic dispersion is given by

$$E_{\mathbf{q}}^2 \simeq \frac{9}{4} q_y^2 a^2 t_2^2 + \frac{3\sqrt{3}}{2} q_x q_y a^2 (t_3^2 - t_1^2) + \frac{3}{4} q_x^2 a^2 (2t_1^2 - t_2^2 + 2t_3^2) + \mathcal{O}(q^3). \quad (2)$$

The Fermi surface is consequently an ellipse, with principal axes that will be rotated with respect to  $\mathcal{O}xy$  in the general situation. eq. (2) can be cast compactly as

$E_{\mathbf{q}}^2 = \hbar^2 v_F^2 \times \mathbf{q} \cdot \boldsymbol{\eta}^2 \cdot \mathbf{q}$ , where  $\hbar v_F \equiv 3ta/2$ . Diagonalization of  $\boldsymbol{\eta}^2$  yields the principal velocities  $v_{\pm}^2 = v_F^2 \eta_{\pm}^2$ , with

$$\eta_{\pm}^2 = \frac{t_1^2 + t_2^2 + t_3^2}{3t^2} \pm \frac{2}{3t^2} \sqrt{t_1^4 + t_2^4 + t_3^4 - t_1^2 t_2^2 - t_2^2 t_3^2 - t_1^2 t_3^2}, \quad (3)$$

and the principal directions:

$$\tan \varphi_{\pm} = \frac{t_3^2 - t_1^2}{\sqrt{3}(\eta_{\pm}^2 t^2 - t_2^2)}. \quad (4)$$

These directions define the slow/longitudinal ( $-, l$ ) and fast/transverse ( $+, t$ ) directions of strained graphene, insofar as the direction-dependent Fermi velocity in the elliptical Fermi surface is smallest along the one, and largest along the other. In the principal coordinate system, the effective Hamiltonian of valley  $\zeta = \pm$  reads

$$H_{\zeta} \simeq \zeta v_F \tau_1 \eta_l p_l + v_F \tau_2 \eta_t p_t, \quad (5)$$

where  $\tau_{1,2}$  are Pauli matrices acting on the ( $A, B$ ) sublattice space. Coupling to a light wave described by the physical vector potential  $\mathbf{A}(t) = \mathbf{A}_0 \exp(-i\omega t)$  is achieved by the minimal substitution  $\mathbf{p} \rightarrow \mathbf{p} + e\mathbf{A}$  in eq. (5). The frequency-dependent conductivity is extracted from the linear response to  $\mathbf{A}_0$ .

For future reference, the anisotropy parameters will be expressed directly in terms of the longitudinal deformation  $\varepsilon$ , to first order. For general tension along  $\theta$  with respect to  $\mathcal{O}x$  we have

$$\eta_t \simeq 1 + a\lambda\nu\varepsilon, \quad \eta_l \simeq 1 - a\lambda\varepsilon, \quad (6a)$$

$$\delta\mathbf{k}_{D,\zeta} \simeq \zeta\lambda\varepsilon \frac{1+\nu}{2} (\cos 2\theta, -\sin 2\theta), \quad (6b)$$

$$\tan \varphi_l \simeq \left[ 1 - a\lambda\varepsilon \frac{1+\nu}{8} (1 + 2\cos 4\theta) \right] \tan \theta, \quad (6c)$$

$$\tan \varphi_t \simeq \left[ 1 + a\lambda\varepsilon \frac{1+\sigma}{8} (1 + 2\cos 4\theta) \right] \tan\left(\theta + \frac{\pi}{2}\right). \quad (6d)$$

As intuition dictates, the slow/longitudinal axis is coincident with the tension axis ( $\varphi \approx \theta$ ). From (5) the strain-induced correction to the density of states (DOS) in the vicinity of the Dirac points follows immediately:  $\rho(E) \simeq \rho^{\text{iso}}(E)/(\eta_l \eta_t)$ , where the isotropic DOS reads  $\rho^{\text{iso}}(E) = 2|E|/(\pi\hbar^2 v_F^2)$ . Notice that, even though the effective longitudinal (transverse) velocity increases (decreases), the net effect in the DOS is always a slope enhancement, because  $\eta_l \eta_t \approx 1 - a\lambda(1 - \nu)\varepsilon < 1$ . This means that strain modifies the Fermi energy and/or electron density.

### III. CONDUCTIVITY OF STRAINED GRAPHENE

Kubo's form of the frequency dependent conductivity reads

$$\sigma_{\alpha\beta}(\omega) = \frac{ig_s q^2}{A\omega} \sum_{\mathbf{k}\lambda\lambda'} \frac{v_\alpha^{\mathbf{k}\lambda\lambda'} v_\beta^{\mathbf{k}\lambda'\lambda} (n_{\mathbf{k}\lambda} - n_{\mathbf{k}\lambda'})}{\hbar\omega - (\epsilon_{\mathbf{k},\lambda'} - \epsilon_{\mathbf{k},\lambda}) + i0^+}, \quad (7)$$

where  $g_s = 2$  is the spin degeneracy,  $A$  the total area,  $\lambda, \lambda' = \pm$ , and  $v_\alpha^{\mathbf{k}\lambda\lambda'} \equiv \langle \mathbf{k}, \lambda | v_\alpha | \mathbf{k}, \lambda' \rangle$  are the matrix elements of the velocity operator  $v_\alpha = i\hbar^{-1}[H, x_\alpha]$  in the momentum eigenbasis. For the general tight-binding Hamiltonian (1), these matrix elements read explicitly

$$\begin{aligned} \langle \mathbf{k}, \lambda | v | \mathbf{k}', \lambda' \rangle &= -\frac{\lambda}{\hbar} \delta_{\mathbf{k}, \mathbf{k}'} \delta_{\lambda\lambda'} \sum_{\alpha} t_\alpha \delta_\alpha \sin[\mathbf{k} \cdot \mathbf{n}_\alpha - \theta_{\mathbf{k}}] \\ &- \frac{i\lambda}{\hbar} \delta_{\mathbf{k}, \mathbf{k}'} (1 - \delta_{\lambda\lambda'}) \sum_{\alpha} t_\alpha \delta_\alpha \cos[\mathbf{k} \cdot \mathbf{n}_\alpha - \theta_{\mathbf{k}}], \end{aligned} \quad (8)$$

with  $\theta_{\mathbf{k}} = \arg[\sum_i t_i \exp(i\mathbf{k} \cdot \mathbf{n}_i)]$ . Contributions with  $\lambda = \lambda'$  are associated with *intra*-band transitions, and  $\lambda \neq \lambda'$  with *inter*-band, direct transitions. In this form the conductivity can be directly calculated at the tight-binding level. In order to proceed fully analytically we work in the Dirac approximation (5), and consider a clean system at zero temperature, thus retaining only the inter-band contribution. In the principal coordinate system defined by the slow/longitudinal and fast/transverse axes the relevant matrix elements become:

$$|v_l^{\mathbf{k}, \lambda, -\lambda}|^2 \approx v_F^2 \eta_t^2 \sin^2 \theta_{\mathbf{k}_D}, \quad (9a)$$

$$|v_t^{\mathbf{k}, \lambda, -\lambda}|^2 \approx v_F^2 \eta_t^2 \cos^2 \theta_{\mathbf{k}_D}, \quad (9b)$$

$$v_l^{\mathbf{k}, \lambda, -\lambda} v_t^{\mathbf{k}, -\lambda, \lambda} \approx \zeta v_F^2 \frac{\eta_l \eta_t}{2} \sin(2\theta_{\mathbf{k}_D}). \quad (9c)$$

The anisotropy is explicitly encoded both in the parameters  $\eta_\pm$ , and in the phase  $\theta_{\mathbf{k}_D}$ .

From here and eq. (7) it is straightforward to obtain the frequency dependent conductivity  $\sigma_{\alpha\beta} = \sigma'_{\alpha\beta} + i\sigma''_{\alpha\beta}$ . Its real part reads

$$\sigma'_{ll}(\omega) \simeq \frac{\eta_l}{\eta_t} \times \sigma_0 \times \left[ f\left(-\frac{\hbar\omega}{2} - \mu\right) - f\left(\frac{\hbar\omega}{2} - \mu\right) \right] \quad (10)$$

for the longitudinal conductivity, and  $\sigma'_{tt}(\omega) = (\eta_t/\eta_l)^2 \sigma'_{ll}(\omega)$  for the transverse component. The isotropic (and universal) value is  $\sigma_0 = e^2/(4\hbar)$ , and  $f(x)$  represents the Fermi-Dirac occupation function. The imaginary part,  $\sigma''(\omega)$ , reads

$$\sigma''_{ll}(\omega) \simeq \frac{\eta_l}{\eta_t} \times \frac{\sigma_0}{\pi} \times \log \left| \frac{2|\mu| - \omega}{2|\mu| + \omega} \right| \quad (11)$$

when  $T = 0$ , and  $\sigma''_{tt}(\omega) = (\eta_t/\eta_l)^2 \sigma''_{ll}$ . The off-diagonal components  $\sigma_{lt}$  are zero, as one expects from symmetry and the absence of magnetic fields. This result shows that  $\sigma'_{ii}(\omega)$  is still constant within the region of validity

of the Dirac approximation, and for  $2\mu \lesssim \hbar\omega \ll T$ , being only renormalized by the anisotropy factors  $\eta_\pm$ . The degree of anisotropy is controlled by  $\eta_l/\eta_t$ , which is a sensible result because  $\sigma_{ii}(\omega) \propto |v_i^{\mathbf{k}, \lambda, -\lambda}|^2$ , and the ratio reflects the quotient between the Fermi velocities along the principal strain directions. From Eqs. (10) and (11), and recalling the expressions in eq. (6a), we can express the strain induced corrections to the full isotropic conductivity,  $\sigma(\omega) = \sigma'(\omega) + i\sigma''(\omega)$ , in linear order in the deformation as

$$\sigma_{ll,tt}(\omega) \simeq \sigma^{\text{iso}}(\omega) \times (1 \mp 2|\delta k_D|a), \quad (12)$$

where  $\sigma^{\text{iso}}(\omega)$  represents the full frequency-dependent conductivity in the absence of strain. For example, tension along  $\mathcal{ZZ}$  ( $\theta = 0$ ) yields a decrease in  $\sigma_{xx}$ , and an increase of the same magnitude for  $\sigma_{yy}$ . Substitution of the material parameters applicable to free-standing graphene in (12) and (6b) yields an anisotropy factor  $(\sigma_t - \sigma_l)/\sigma^{\text{iso}} = 4|\delta k_D|a \sim 8\epsilon$ . This is sufficiently marked to be detectable by conventional optical means, like absorption in the visible or IR, which we discuss below.

### IV. AB-INITIO OPTICAL CONDUCTIVITY

Given the approximations used, it is legitimate to question the validity of the analytical corrections written in eq. (12). To that end, we have extracted the optical conductivity of uniaxially strained graphene from first-principles as well. Density Functional Theory (DFT) calculations were performed with the *ab-initio* spin-density functional code AIMPRO [27]. We used the GGA in the scheme of Perdew, Burke, and Ernzerhof [28]. Core states were accounted for by dual-space separable pseudopotentials [29]. The valence states are expanded over a set of  $s$ ,  $p$ , and  $d$ -like localized, atom-centered Gaussian functions. The BZ was sampled according to the scheme proposed by Monkhorst-Pack [30]. We used a convergence-tested grid of  $20 \times 20 \times 1$  points for the self-consistent calculations. In equilibrium we obtained the optimized lattice parameter  $a = 1.42 \text{ \AA}$ .

Uniaxial strain was applied with relaxation as described earlier in Ref. 24. For each strained configuration we extracted the dielectric function within the long-wavelength dipole approximation [31], and from it the optical conductivity. The results for  $\sigma'_{xx}(\omega)$  and  $\sigma'_{yy}(\omega)$  so obtained are shown in fig. 2, for representative uniaxial strains applied along  $\mathcal{ZZ}$  ( $\theta = 0$ ) and  $\mathcal{AA}$  ( $\theta = \pi/2$ ).

The main panel of fig. 2(a) shows the renormalization of the real part of  $\sigma_{xx}$ , which corresponds to  $\sigma_{ll}$  for  $\mathcal{ZZ}$  and  $\sigma_{tt}$  for  $\mathcal{AA}$ . It is clear that for visible and IR frequencies the conductivity remains roughly constant in  $\omega$ , but its magnitude depends on the amount of strain. The strain dependence is shown in detail in the inset, at  $\omega = 1 \text{ eV}$ . The perfect linearity in  $\epsilon$  of the *ab-initio* results up to at least  $\epsilon \approx 10\%$  shows that the analytical result of eq. (12) is indeed quite dependable for a

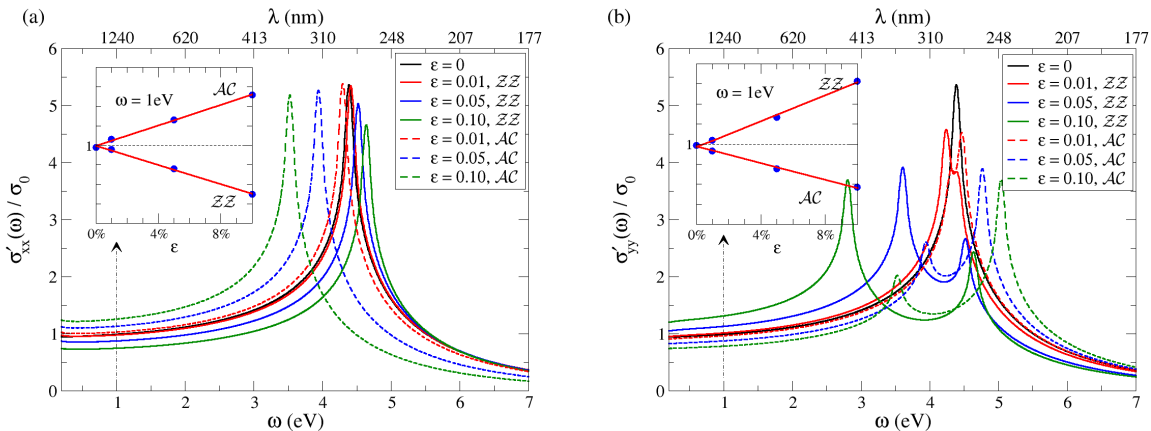


FIG. 2: Real part of the optical conductivity  $\sigma_{xx}$  (a) and  $\sigma_{yy}$  (b), calculated *ab-initio* for graphene under uniaxial strain along  $\mathcal{ZZ}$  ( $\theta = 0$ ) and  $\mathcal{AA}$  ( $\theta = \pi/2$ ). The sharp absorption peaks are associated with transitions resonant with the van Hove singularities. In panel (a) the peak is resonant with the transition at  $M_{1,3}$  in the BZ, whereas in panel (b) the double peak structure derives from the splitting between transitions at  $M_{1,3}$  and  $M_2$ . Both insets show the variation of  $\sigma'_{ii}$  with strain at  $\omega = 1$  eV, as obtained *ab-initio*. The straight lines are linear fits, which yield slopes of  $-2.45$  ( $\mathcal{ZZ}$ ) and  $2.64$  ( $\mathcal{AA}$ ) for the inset of panel (a), and  $3.22$  ( $\mathcal{ZZ}$ ) and  $-2.08$  ( $\mathcal{AA}$ ) for the inset of panel (b).

wide range of stretching. We must point out, however, that the linear slopes quoted in fig. 2 cannot immediately be used to extract the bandstructure parameter  $\lambda$  using eq. (12). That is because the *ab-initio* calculation naturally includes the relaxation and deformation of the lattice, which, as advanced in the very beginning, we chose to ignore, not to encumber the discussion by more complicated expressions which do not change the main results.

Taking the lattice deformation into account leads to a correction of the expansion (2) of the dispersion around the Dirac points. This leads to a renormalization of entries in the matrix  $\boldsymbol{\eta}^2$ . It can be shown straightforwardly that such changes amount to replacing  $\lambda a \rightarrow \lambda a - 1$  in  $\boldsymbol{\eta}^2$ , and, consequently, in every ensuing result. In this way, the *ab-initio* slopes quoted in fig. 2 correspond to  $\lambda \simeq 2.42 \text{ \AA}^{-1}$  ( $\mathcal{ZZ}$ ) and  $\lambda \simeq 2.56 \text{ \AA}^{-1}$  ( $\mathcal{AA}$ ) for the inset of panel (a), and  $\lambda \simeq 2.97 \text{ \AA}^{-1}$  ( $\mathcal{ZZ}$ ) and  $\lambda \simeq 2.17 \text{ \AA}^{-1}$  ( $\mathcal{AA}$ ) for the inset of panel (b). This rather nicely agrees with the estimates quoted earlier that put  $\lambda a \sim 3 - 4$ .

## V. VAN HOVE SINGULARITIES

In the UV band,  $\sigma(\omega)$  is dominated by direct transitions between the  $M$  points in the BZ, which coincide with VHS in the electronic dispersion. From the point of view of (1), these transitions occur at momenta  $\mathbf{k}$  coinciding precisely with  $M_{1,3} = (\pm\pi/\sqrt{3}, \pi/3)$  and  $M_2 = (2\pi/3, 0)$  (see fig. 1 for our convention regarding the  $M$  points). The corresponding resonant frequencies are therefore given by  $\omega_{M_i} = 2|E(\mathbf{k} = M_i)|$ , and read  $\omega_{M_1} = 2|t_1 + t_2 - t_3|$ ,  $\omega_{M_2} = 2|t_1 - t_2 + t_3|$ , and

$\omega_{M_3} = 2| -t_1 + t_2 + t_3|$ . In the most general situation  $t_1 \neq t_2 \neq t_3$  the VHS split. Linearly expanding the hoppings in the magnitude of uniaxial strain, and defining  $\omega_{M_i} \approx 2t + ta\lambda\varepsilon\Delta\omega_{M_i}$ , such splitting acquires the explicit form

$$\Delta\omega_{M_{1,3}} \simeq \nu - 1 + (1 + \nu)(\cos 2\theta \pm \sqrt{3}\sin 2\theta), \quad (13a)$$

$$\Delta\omega_{M_2} \simeq \nu - 1 - 2(1 + \nu)\cos 2\theta. \quad (13b)$$

But, as is obvious from the *ab-initio* results in fig. 2, this splitting is not always visible in the absorption spectrum. That is because the velocity matrix elements (8) impose a modulation of the strength associated with these transitions. In order to extract this effect we need to abandon the Dirac approximation (5,9), and work with the full-tight binding bandstructure and matrix elements. In (8) take, for example, the matrix elements at  $\mathbf{k} = M_2$ , which read

$$|v_x^{M_2}|^2 = \frac{3a^2}{4\hbar^2}(t_1 - t_3)^2, \quad (14a)$$

$$|v_y^{M_2}|^2 = \frac{1a^2}{4\hbar^2}(t_1 + 2t_2 + t_3)^2, \quad (14b)$$

$$v_x^{M_2}v_y^{M_2} = -\frac{\sqrt{3}a^2}{4\hbar^2}(t_1 + 2t_2 + t_3)(t_1 - t_3). \quad (14c)$$

When expanded in powers of strain,  $|v_x^{M_2}|^2$  will be zero to linear order, irrespective of the strain direction. This suppresses the  $M_2$  singularity in  $\sigma'(\omega)$  leaving only the peaks related to  $M_{1,3}$ , whose associated matrix elements are finite. Since the geometry chosen in fig. 2 considers only  $\theta = 0$  and  $\pi/2$ ,  $M_1$  and  $M_3$  are still degenerate, as per (13), and thus only one peak should survive in  $\sigma'_{xx}$ , precisely as seen *ab-initio* in fig. 2(a). On the

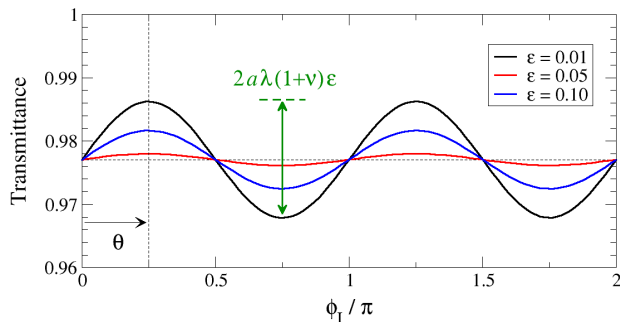


FIG. 3: Illustration of the behavior of the transmittance as a function of incident polarization measured in the laboratory frame. According to (16), the phase shift  $\theta$  defines the direction of strain, and the amplitude its magnitude.

other hand, there is no such selection rule arising from the velocity matrix elements when computing  $\sigma'_{yy}$ , which allows the splitting between  $M_2$  and  $M_{1,3}$  to be observed, as fig. 2(b) clearly demonstrates. Eqs. (13) also explain why in fig. 2(a) the strain-induced shift of the peak is less pronounced for tension along  $\mathcal{ZZ}$  ( $\theta = 0$ ), than  $\mathcal{AA}$  ( $\theta = \pi/2$ ):  $\Delta\omega_{M1}(\mathcal{ZZ}) = \nu \Delta\omega_{M1}(\mathcal{AA})$ . And similarly, Eqs. (14) account for the different relative intensity of the peaks associated with  $M_2$  and  $M_{1,3}$  in fig. 2(b).

It is important to stress here that these results are not tied to a particular coordinate system. We can easily express Eqs. (14) in any coordinate system, rotated by  $\varphi$  with respect to  $\mathcal{O}xy$ , and conclude that the longitudinal matrix element  $|v_{x'}^{M_i}|^2$  always vanishes when  $\varphi$  coincides with a  $\mathcal{ZZ}$  direction. For example,  $|v_{x'}^{M_2}|^2$  vanishes for  $\varphi = 0$ ,  $|v_{x'}^{M_3}|^2$  vanishes for  $\varphi = \pi/3$ , and  $|v_{x'}^{M_1}|^2$  vanishes for  $\varphi = 2\pi/3$ . Suppression of a van Hove peak in the longitudinal conductivity therefore singles out one of the  $\mathcal{ZZ}$  directions of the lattice. This is consistent and explains the numerical calculations of Ref. 21, and has an important consequence: by monitoring the splitting in the absorption peaks associated with VHS, and by inspecting the selection rule just described, *one can measure simultaneously: the magnitude of strain, its direction, and the direction of the underlying lattice with respect to the laboratory coordinate system*. This provides an optical means to perform the same measurements that have been made by exploring the splitting of the  $G$  peak in the Raman spectrum of strained graphene [32, 33].

## VI. TRANSPARENCY AND DICHROISM

The asymmetry (12) in the conductivity tensor will result in a certain degree of dichroism, as the absorbance of linearly polarized light will depend on the polarization direction with respect to the slow/fast axes. Treating graphene as a 2D conducting sheet, and solving the associated Fresnel equations, we can extract the degree of polarization rotation for normal incidence on graphene in vacuum. In the visible and IR where eq. (12) stands

that would be

$$\frac{\tan \phi_T}{\tan \phi_I} = \frac{2 + c\mu_0\sigma_{ll}}{2 + c\mu_0\sigma_{tt}} \approx 1 - 4|\delta k_D|a \frac{c\mu_0\sigma_0}{2 + c\mu_0\sigma_0}, \quad (15)$$

where  $\phi_{T,I}$  are the transmitted and incident polarizations measured with respect to the slow/longitudinal axis, and  $c\mu_0\sigma_0 = \pi\alpha \approx 0.02$ . Likewise, the transmittance for linear polarization becomes

$$\mathcal{T} \approx 1 - \pi\alpha [1 - 2|\delta k_D|a \cos 2\phi_I] \quad (16)$$

An important consequence of this periodic modulation is that it allows a direct determination of both the strain direction and its magnitude, as follows. In some laboratory coordinates (16) is transformed by making  $\phi_I \rightarrow \phi_I - \varphi_I$ . The amplitude of  $\mathcal{T}$  as a function of polarization direction determines the amount of strain, while the phase shift  $\varphi_I$  fixes the direction. This is illustrated in fig. 3. The corrections to both polarization and transmittance are weighted by  $\pi\alpha$ , and will be necessarily small. But, on the one hand, the modulation amplitude is roughly  $\sim 8\varepsilon\pi\alpha$  ( $0.16\varepsilon$ ) and transmittance can be routinely measured within 0.1% of precision. On the other hand, the transmittance of multilayer graphene is, to a great extent, cumulative [1, 7]. This implies that the same results apply for multilayer graphene, provided one replaces  $\pi\alpha \rightarrow N\pi\alpha$  in (16), where  $N$  accounts for the number of graphene layers. The effect is thus naturally enhanced in multilayers, as it is in the vicinity of the VHS (or any resonance, for that matter). Another interesting application is that, if strain can be controlled with precision, an expression like (16) allows, by means of a simple optical experiment, the measurement of the bandstructure parameter  $\lambda = d \log t / dr$ , whose knowledge is crucial for the characterization of all strain-induced effects on the bandstructure.

## VII. DISCUSSION

The photoelastic effect in undoped graphene has been quantified, and shown to possess features that might be appealing in the development of atomically thin optical elements. One of such characteristics is the frequency independent response in a very large frequency range, which remains valid when the system is anisotropically strained. This constancy and predictability is a relevant feature for broadband applications. The degree of anisotropy induced by strain is determined by how much the Dirac point is displaced from its position at  $K/K'$  in the BZ:  $|\delta k_D|$  (6b). This opens several possibilities, such as: monitoring optical absorption as a function of strain to characterize the band parameters of graphene; or monitoring the transmittance as a function of incident polarization in order to measure the magnitude and direction of strain in graphene devices. This last example could find applications in completely passive, transparent, strain sensors.

Even if the magnitude of the photoelastic effect in graphene at visible or IR frequencies is limited by its small natural absorption of  $\pi\alpha \sim 2\%$ , it is nonetheless significant for an atomically thin membrane. Additional versatility is provided by the fact that the effect can be naturally amplified by stacking multilayers, or that the optical absorption can be radically affected by electronic doping as well, on account of Pauli blocking [5, 9].

A determination of the lattice orientation cannot be made from the optical absorption at low energies, simply due to the isotropy of the Dirac dispersion. By contrast, the electronic dispersion at energies close to the VHS fully reflects the symmetry of the underlying lattice. Therefore, by measuring the optical response at frequencies resonant with the van Hove transitions, and analyzing the strain-induced splitting and selection rules of the absorption peaks, one can extract the amount of strain, its direction, and the lattice orientation.

Another consequence of the strain-induced tunability of the VHS is that it can have a significant import in current efforts to elevate the Fermi level of graphene up to the VHS [34–36]. The ability to achieve this, and thereby dramatically increase the electronic DOS, is expected to facilitate many-body instabilities and the establishment of correlated phases, such as superconductivity, or charge/spin density waves [37, 38]. Strain engineering of

graphene can, in this respect, work as a facilitator and provide added tunability. For example, from (13) it follows that the energy of the VHS can be reduced by uniaxial strain to values as low as  $E/t \simeq 1 - (3+\nu)a\lambda\varepsilon/2$ . Using  $\lambda a \sim 3$  for estimate purposes we can write  $E/t \simeq 1 - 5\varepsilon$ , so that the reduction for 10% strain can be as much as 50% in the position of the VHS. On top of this we would need to include excitonic corrections that are known to renormalize the VHS further down in energy [39], and which we neglect in our treatment.

Finally, the photoelastic effect is the basis of many optical and mechano-optical devices and applications at the macro-scale. The characteristics of graphene in this respect, which we just surfaced, might provide a valuable route towards the downscaling of those concepts to the realm of atomically thin optical elements, and their application at the nanoscale.

### Acknowledgments

AHCN acknowledges the partial support of the U.S. DOE under grant DE-FG02-08ER46512, and ONR grant MURI N00014-09-1-1063.

- 
- [1] R. R. Nair, P. Blake, A. N. Grigorenko, K. S. Novoselov, T. J. Booth, T. Stauber, N. M. R. Peres, and A. K. Geim, *Science* **320**, 1308 (2008).
- [2] K. Bolotin *et al.*, *Solid State Comm.* **146**, 351 (2008).
- [3] X. Li, Y. Zhu, W. Cai, M. Borysiak, B. Han, D. Chen, R. D. Piner, L. Colombo, and R. S. Ruoff, *Nano Lett.* **9**, 4359 (2009).
- [4] S. Bae, H. K. Kim, X. Xu, J. Balakrishnan, T. Lei, Y. I. Song, Y. J. Kim, B. Ozyilmaz, J.-H. Ahn, B. H. Hong, *et al.*, *Nature Nano.* **5**, 574 (2010).
- [5] Z. Q. Li, E. A. Henriksen, Z. Jiang, Z. Hao, M. C. Martin, P. Kim, H. L. Stormer, and D. N. Basov, *Nature Physics* **4**, 532 (2008).
- [6] K. F. Mak, M. Y. Sfeir, Y. Wu, C. H. Lui, J. A. Misewich, and T. F. Heinz, *Phys. Rev. Lett.* **101**, 196405 (2008).
- [7] A. B. Kuzmenko, E. van Heumen, F. Carbone, and D. van der Marel, *Phys. Rev. Lett.* **100**, 117401 (2008).
- [8] K. F. Mak, M. Y. Sfeir, J. A. Misewich, and T. F. Heinz, *Proc. Nat. Acad. Sci.* **107**, 14999 (2010).
- [9] T. Ando, Y. Zheng, and H. Suzuura, *J. Phys. Soc. Jpn.* **71**, 1318 (2002).
- [10] N. M. R. Peres, F. Guinea, and A. H. Castro Neto, *Phys. Rev. B* **73**, 125411 (2006).
- [11] L. A. Falkovsky and A. A. Varlamov, *Eur. Phys. J. B* **56**, 281 (2007).
- [12] E. G. Mishchenko, *Phys. Rev. Lett.* **103**, 246802 (2009).
- [13] D. E. Sheehy and J. Schmalian, *Phys. Rev. B* **80**, 193411 (2009).
- [14] V. P. Gusynin, S. G. Sharapov, and J. P. Carbotte, *New J. Phys.* **11**, 095013 (2009).
- [15] N. M. R. Peres, R. M. Ribeiro, and A. H. Castro Neto, *Phys. Rev. Lett.* **105**, 055501 (2010).
- [16] A. H. Castro Neto, F. Guinea, N. M. R. Peres, K. S. Novoselov, and A. K. Geim, *Rev. Mod. Phys.* **81**, 109 (2009).
- [17] N. M. R. Peres, *Rev. Mod. Phys.* **82**, 2673 (2010).
- [18] V. M. Pereira and A. H. Castro Neto, *Phys. Rev. Lett.* **103**, 046801 (2009).
- [19] F. Guinea, M. I. Katsnelson, and A. K. Geim, *Nature Physics* **6**, 30 (2010).
- [20] F. M. D. Pellegrino, G. G. N. Angilella, and R. Pucci, *High. Press. Res.* **29**, 569 (2009).
- [21] F. M. D. Pellegrino, G. G. N. Angilella, and R. Pucci, *Phys. Rev. B* **81**, 035411 (2010).
- [22] A. Sinner, A. Sedrakyan, and K. Ziegler (2010), arXiv:1010.4510.
- [23] V. M. Pereira, N. M. R. Peres, and A. H. Castro Neto, *Phys. Rev. B* **80**, 045401 (2009).
- [24] R. M. Ribeiro, V. M. Pereira, N. M. R. Peres, P. R. Briddon, and A. H. Castro Neto, *New J. Phys.* **11**, 115002 (2009).
- [25] Z. H. Ni, T. Yu, Y. H. Lu, Y. Y. Wang, Y. P. Feng, and Z. X. Shen, *ACS Nano* **3**, 483 (2009).
- [26] S.-M. Choi, S.-H. Jhi, and Y.-W. Son, *Phys. Rev. B* **81**, 081407(R) (2010).
- [27] M. J. Rayson and P. R. Briddon, *Comput. Phys. Commun.* **178**, 128 (2008).
- [28] J. P. Perdew, K. Burke, and M. Ernzerhof, *Phys. Rev. Lett.* **77**, 3865 (1996).
- [29] C. Hartwigsen, S. Goedecker, and J. Hutter, *Phys. Rev. B* **58**, 3641 (1998).
- [30] J. D. P. H. J. Monkhorst, *Phys. Rev. B* **13**, 5188 (1976).

- [31] C. J. Fall *et al.*, Phys. Rev. B **65**, 205206 (2008).
- [32] T. M. G. Mohiuddin, A. Lombardo, R. R. Nair, A. Bonetti, G. Savini, R. Jalil, N. Bonini, D. M. Basko, C. Galiotis, N. Marzari, et al., Phys. Rev. B **79**, 205433 (2009).
- [33] M. Huang, H. Yan, C. Chen, D. Song, T. F. Heinz, and J. Hone, Proc. Nat. Acad. Sci. **106**, 7304 (2009).
- [34] A. Pachoud, M. Jaiswal, P. K. Ang, K. P. Loh, and B. Oezylmaz, EPL **92**, 27001 (2010).
- [35] D. K. Efetov and P. Kim (2010), arXiv:1009.2988.
- [36] J. T. Ye, M. F. Craciun, M. Koshino, S. Russo, S. Inoue, H. T. Yuan, H. Shimotani, A. F. Morpurgo, and Y. Iwasa (2010), arXiv:1010.4679.
- [37] J. González, Phys. Rev. B **78**, 205431 (2008).
- [38] J. L. McChesney, A. Bostwick, T. Ohta, T. Seyller, K. Horn, J. González, and E. Rotenberg, Phys. Rev. Lett. **104**, 136803 (2010).
- [39] L. Yang, J. Deslippe, C.-H. Park, M. L. Cohen, and S. G. Louie, Phys. Rev. Lett. **103**, 186802 (2009).